Thermomechanical Behavior of TiNi Shape Memory Alloy Fiber Reinforced 6061 Aluminum Matrix Composite

K. HAMADA, J.H. LEE, K. MIZUUCHI, M. TAYA, and K. INOUE

The processing and thermomechanical behaviors of TiNi shape memory alloy (SMA) fiber-reinforced 6061 Al matrix smart composites are investigated experimentally and analytically. Optimum processing conditions of hot pressing temperature and pressure are identified. Composite yield stresses are observed to increase with an increase in the volume fraction of TiNi fiber and prestrain given to the composites. An analytical model for thermomechanical behavior of the composites is developed by utilizing an exponential type of SMA constitutive model. The model predicts an increase in the composite yield stress with an increase in prestrain. It is found that the key parameters affecting the composite yield stress are the fiber volume fraction, prestrain, and matrix heat treatment. The predictions are in a reasonably good agreement with the experimental results.

I. INTRODUCTION

SMART composites that utilize shape memory alloy (SMA) fibers as reinforcement have been designed and successfully developed.[1–5] The design concept of smart composite is shown in Figure 1. The SMA fibers are loaded at room temperature transforming the austenitic phase to the martensitic phase. Then they are heated to induce the reverse transformation. The SMA fibers in a composite shrink during this reverse transformation, which induces tensile stress in fibers and compressive stress in the matrix. This compressive stress in the matrix is a key factor that enhances the tensile properties of a smart composite. The internal stress analysis is the critical step for precise evaluation of the smart composite.

Recently, we developed two types of smart composite utilizing TiNi fiber as a reinforcement, namely, TiNi/Al and TiNi/epoxy. We succeeded in improving both the yield stress of TiNi/Al and the fracture toughness of TiNi/epoxy at high temperatures.[1,3,5] We used a pure Al for the composite matrix as it can be processed easily.[3] However, a pure Al matrix is not ideal for applications of smart composites to structural composites due to its low yield stress. Hence, the present study uses a 6061 Al alloy in its T6 heat treatment. In addition, we use a vacuum hot press method to enhance strong interfacial bonding between TiNi fibers and matrix for the present processing, while pressure casting of molten Al matrix was used in the previous experiments.[3]

Our previous model predicted that the martensite phase induced in prestrain process shows reverse transformation to austenite above A_f at high temperature, leaving the TiNi fiber fully austenite.[1] In this article, we develop a model that includes the stress effects on the phase transformation during the heating process, because the phase transformation is strongly affected by both temperature and stress.[6] Boyd and Lagoudas[2] analyzed the elastic behavior of a TiNi/elastomer composite utilizing the Mori–Tanaka micromechanics method[7] and one-dimensional model of SMA transformation.[8] However, these researchers did not compare predicted values to experimental results. Armstrong and Kino[9] and Armstrong[10] reported predictions and experimental data on the thermomechanical behavior of a TiNi/6061 Al composite. Although their one-dimensional thermomechanical model included the matrix yielding, they did not focus on the enhancement of composite yield stress.

The objectives of this article are threefold: to identify the best processing condition of TiNi/6061 Al composite; to demonstrate the enhanced mechanical performance of the composite at high temperatures; and to develop a one-dimensional model for more accurate stress analysis of the composites under thermomechanical loading.

II. EXPERIMENTAL PROCEDURE

The Ti-50.3 at. pct Ni SMA fibers of 200 μm in diameter are used. The TiNi fibers are heat treated at 773 K in air for 30 minutes and quenched into water for shape memorization. In order to obtain mechanical properties and transformation data, fiber tensile tests are performed at various temperatures between 297 to 373 K in air at a constant strain rate of 1×10^{-4}/s with 30-mm gage length. Stress-strain curves of TiNi fibers indicate that the transformation temperatures increase with applied stress. The transformation starting stress and finishing stress for a given temperature can be obtained based on these curves, and a differential scanning calorimeter is used to measure transformation temperatures without stress. Based on these results, a phase transformation stress–temperature diagram is constructed and shown in Figure 2.

A vacuum hot press method under 10^{-2} torr condition is used for processing. To keep the fibers aligned and to prevent them from contacting each other, a method developed by Armstrong and Kino[9] is modified. The TiNi fibers are

K. HAMADA, formerly Research Associate, Department of Mechanical Engineering, University of Washington, is currently Research Associate, Department of Dental Eng., School of Dentistry, Tokushima University, Tokushima-City, 770-8504, Japan. M. TAYA, Professor, Department of Mechanical Engineering, and K. INOUE, Professor, Department of Materials Science and Engineering, are with the University of Washington, Seattle, WA 98195. J.H. LEE, Professor, Department of Metallurgical Engineering, Dong-A University, Pusan 604-714, Korea, is Visiting Professor, Department of Materials Science and Engineering, University of Washington. K. MIZUUCHI is Senior Researcher with the Osaka Municipal Technical Research Institute, Osaka 536, Japan.

Manuscript submitted February 18, 1997.

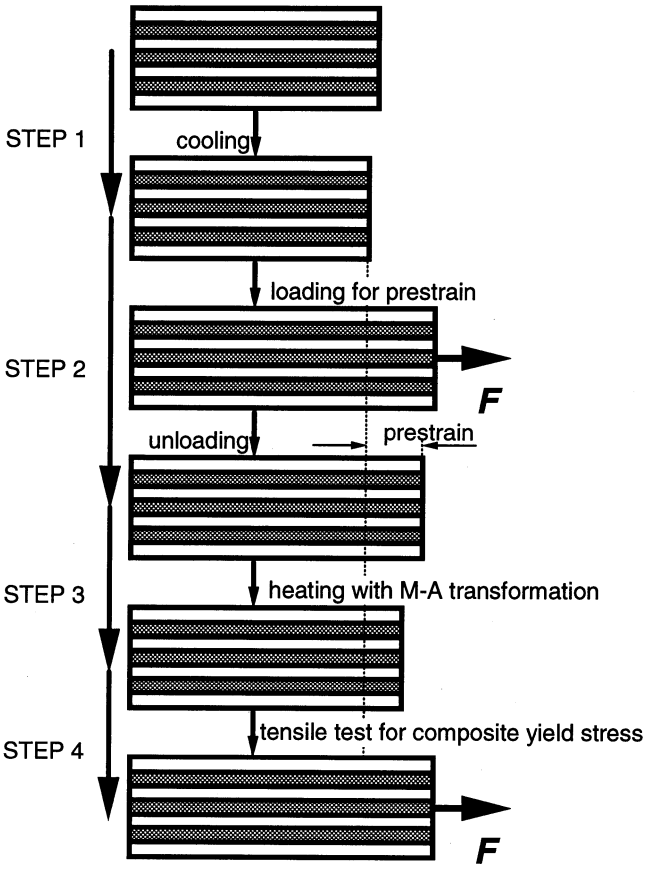

Fig. 1—Design concept of a smart composite.

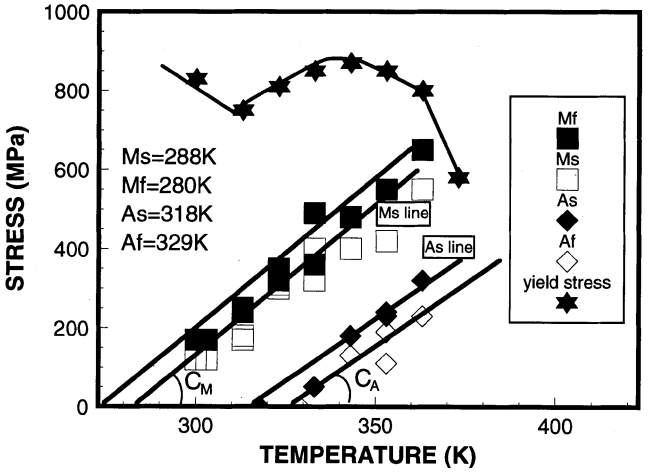

Fig. 2—Stress-temperature diagram of a TiNi shape memory fiber.

wound around 90 × 10-mm 6061 Al sheets at constant spacing, and these prepreg sheets are stuck between the press dies, as shown in Figure 3. Two different volume fractions of TiNi fibers are in our experiment: 2.7 and 5.3 pct. To optimize the processing condition of composites, specimens are processed under three different temperatures and pressures with a constant pressing time of 30 minutes. The processing temperature is measured on the press die surface, and the press pressure is calculated based on the original size of Al sheet before pressing. Cross-sectional views of the composites processed under various conditions are summarized in Figure 4. Figure 4 indicates that the

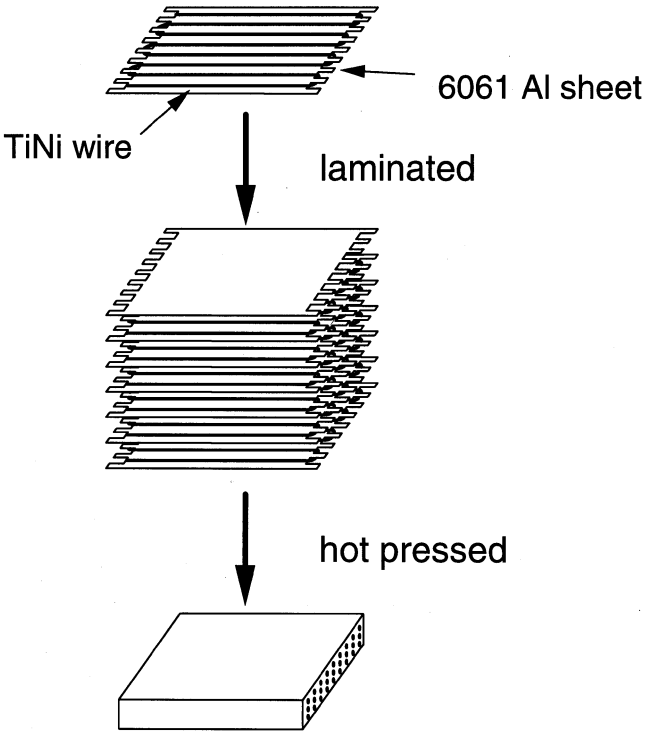

Fig. 3—Prepreg setting for a vacuum hot press.

strong bonding between fiber and matrix can be obtained by using the processing condition of 873 K (600 °C) at 7 MPa and 823 K (550 °C) at 14 MPa, but the bond lines between the original Al sheets cannot be eliminated. On the other hand, the gap and bond lines are eliminated when processed at 773 K (500 °C) at 54 MPa. As the surface of Al sheets can be oxidized easily in air, a large plastic flow due to high pressure is required for breaking the oxidized surface layer, resulting in a stronger bonding of Al sheets. The hot pressing is, therefore, performed at 773 K for 30 minutes at 54 MPa, and specimens are cooled down in the furnace. Flat bar type tensile specimens are cut out from as-processed composite plate (Figure 5). To enhance the yield strength of the matrix, T6 heat treatment is used: specimens are heat treated at 803 K in air for 30 minutes, quenched into water for solution treatment, then heat treated at 443 K in air for 18 hours followed by another water quenching for aging treatment. The water temperature is kept higher than 293 K to keep TiNi fibers in the austenite phase.

As the final step of the processing, the specimens were prestrained at 293 K in air at a strain rate of 1×10^{-4}/s. Mechanical testing at the same strain rate of 1×10^{-4}/s is then conducted on the prestrained specimens at 373 K. Specimen temperature is measured on the surface of the specimen by thermocouples, while the displacement of the specimen is measured by an extensometer with gage length of 10 mm.

III. ANALYTICAL MODELING

A. *One-Dimensional Composite Model*

Under the assumption of isostrain, *i.e.*, no sliding between the fiber and the matrix, we have

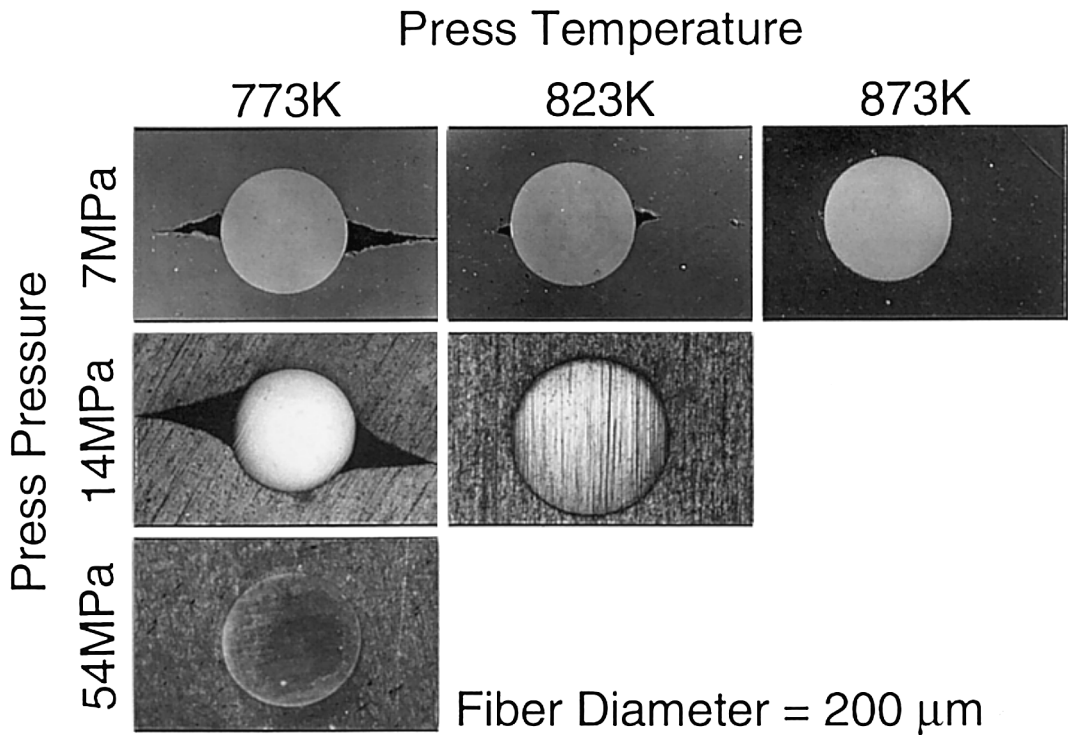

Fig. 4—Effects of temperature and press pressure on bonding conditions between the fiber and matrix of the TiNi/6061 Al composite.

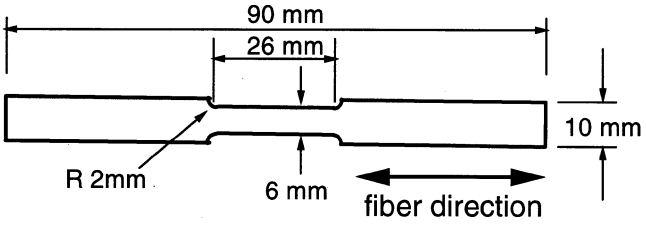

Fig. 5—Dimension of the tensile test specimen.

$$\varepsilon_c = \varepsilon_f = \varepsilon_m \quad [1]$$

where ε_c, ε_f, and ε_m are the total strain of composite, fiber, and matrix, respectively. The force equilibrium equation of a composite along the fiber axis direction renders

$$\sigma_c = V_f \times \sigma_f + (1 - V_f) \times \sigma_m \quad [2]$$

where σ_c is the applied stress of a composite; σ_f and σ_m are the stress of fiber and matrix, respectively; and V_f is the volume fraction of fiber.

As the fiber is not expected to yield in our experiment, the total strain of fiber can be described as

$$\varepsilon_f = \varepsilon_f^{el} + \varepsilon_f^{\text{CTE}} + \varepsilon_f^{\text{trans}} \quad [3]$$

where ε^{el}, ε^{CTE}, and $\varepsilon^{\text{trans}}$ are the elastic strain, thermal strain, and transformation strain, respectively. The matrix strain consists of the elastic (ε_m^{el}), thermal ($\varepsilon_m^{\text{CTE}}$), and plastic strains ($\varepsilon_m^{pl}$):

$$\varepsilon_m = \varepsilon_m^{el} + \varepsilon_m^{\text{CTE}} + \varepsilon_m^{pl} \quad [4]$$

The elastic constitutive equations of fiber and matrix are given by

$$\sigma_f = E_f \times \varepsilon_f^{el} \quad [5]$$

$$\sigma_m = E_m \times \varepsilon_m^{el} \quad [6]$$

where E_f and E_m are the elastic modulus of fiber and matrix, respectively.

The thermal strain can be described as a function of temperature change, dT, as follows:

$$\varepsilon_f^{\text{CTE}} = \alpha_f \times dT \quad [7]$$

$$\varepsilon_m^{\text{CTE}} = \alpha_m \times dT \quad [8]$$

where α_f and α_m are the coefficient of thermal expansion (CTE) of fiber and matrix, respectively.

The work hardening behavior of the matrix metal can be approximated by the following power-law type:

$$\sigma_m = \sigma_{my} + K \times (\varepsilon_m^{pl})^n \quad [9]$$

where σ_{my} is the yield stress of matrix Al and K and n are material constants. From Eqs. [4], [6], [8], and [9], the incremental matrix strain can be obtained by [9]

$$d\varepsilon_m = \frac{d\sigma_m}{E_m} + \frac{d\sigma_m}{nK}\left(\frac{\sigma_m - \sigma_{my}}{K}\right)^{\frac{n-1}{n}} + \alpha_m \times dT \quad [10]$$

B. *Phase Transformation of Shape Memory Fiber*

It is well known that the volume fraction of martensites in an SMA mainly depends on the stress state and temperature. Different types of equations have been proposed to describe the thermomechanical behavior of SMAs.[8–13] Tanaka[8] suggested exponential type equations, and Liang and Rogers[11] used cosine types. In this study, we use the exponential type equations because they better fit the experimental stress-strain curves of the TiNi fiber used. Brinson[12] and Ford and White[13] suggested a modification

assuming that the martensites in a SMA can be divided into thermal and athermal (stress-induced) martensites. In this study, however, we need not use the modified model, because we can assume the martensite in the TiNi fiber used is fully athermal by keeping the temperature of the TiNi fiber above M_s.

The volume fraction of martensite (ξ) during the martensite transformation is defined as follows:[8]

$$\xi(T, \sigma_f) = 1 - \exp\left[a^M \times (M_s - T) + b^M \times \sigma_f\right] \quad [11]$$

$$a^M = \frac{\ln(0.01)}{M_s - M_f}, \quad b^M = \frac{a^M}{C_M} \quad [12]$$

where M_s and M_f are the starting and finishing temperatures of the martensite transformation without stress, respectively, and C_M is the slope of the martensite transformation contours (Figure 2). The end of the martensite transformation is defined as $\xi = 0.99$ (due to the singular behavior in the constitutive equation, $\xi = 1$ was avoided). From Eq. [11], the increment in ξ can be expressed in terms of the increment of T and σ_f by

$$\begin{aligned} d\xi(T, \sigma_f, dT, d\sigma_f) = {} & \exp\left[a^M \times (M_s - T) \right. \\ & \left. + b^M \times \sigma_f\right] \\ & - \exp\left[a^M \times (M_s - T \right. \\ & \left. - dT) + b^M \times (\sigma_f + d\sigma_f)\right] \end{aligned} \quad [13]$$

For the reverse transformation, ξ is given[8] by

$$\xi(T, \sigma_f) = \exp\left[a^A \times (A_s - T) + b^A \times \sigma_f\right] \quad [14]$$

$$a^A = \frac{\ln(0.01)}{A_s - A_f}, \quad b^A = \frac{a^A}{C_A} \quad [15]$$

where A_s and A_f are the starting and finishing temperatures of the reverse transformation without stress, respectively, and C_A is the slope of the reverse transformation contours. Here, the end of the reverse transformation is defined as $\xi = 0.01$. From Eq. [14], the increment in ξ can be expressed in terms of the increment of T and σ_f by

$$\begin{aligned} d\xi(T, \sigma_f, dT, d\sigma_f) = {} & \exp\left[a^A \times (A_s - T - dT) \right. \\ & \left. + b^A \times (\sigma_f + d\sigma_f)\right] \\ & - \exp\left[a^A \times (M_s - T) \right. \\ & \left. + b^A \times \sigma_f\right] \end{aligned} \quad [16]$$

The elastic modulus and the coefficient of thermal expansion of SMAs are known to depend on the martensite volume fraction, ξ. Assuming a linear dependence of α_f and E_f on ξ, we have

$$\begin{aligned} \alpha_f(\xi) &= \xi \times \alpha_f^{\mathrm{MAR}} + (1 - \xi) \times \alpha_f^{\mathrm{AUS}} \\ &= \alpha_f^{\mathrm{AUS}} + \xi \times (\alpha_f^{\mathrm{MAR}} - \alpha_f^{\mathrm{AUS}}) \end{aligned} \quad [17]$$

$$\begin{aligned} E_f(\xi) &= \xi \times E_f^{\mathrm{MAR}} + (1 - \xi) \times E_f^{\mathrm{AUS}} \\ &= E_f^{\mathrm{AUS}} + \xi \times (E_f^{\mathrm{MAR}} - E_f^{\mathrm{AUS}}) \end{aligned} \quad [18]$$

where α_f^{MAR} and α_f^{AUS} are coefficients of thermal expansion of martensite and austenite, respectively, and E_f^{MAR} and E_f^{AUS} are elastic moduli of martensite and austenite, respectively.

The phase transformation strain of SMA fiber is assumed to be a linear function of the martensite volume fraction change, $d\xi$, by

$$d\varepsilon_f^{\mathrm{trans}} = d\xi \times \varepsilon^{t\max} \quad [19]$$

where $\varepsilon^{t\max}$ is the maximum transformation strain from one single phase to the other.

C. *Thermomechanical Process of Smart Composite*

The thermomechanical process of a smart composite can be divided into four steps, as shown in Figure 1. Step 1 is the cooling process after processing or the heat treatment. In this step, there is no applied stress to the composite. Step 2 is the isothermal loading and unloading to provide a given prestrain. Step 3 is the heating process from room temperature to the test temperature without applied stress. Step 4 is the isothermal tensile test.

During steps 1 and 3, where there is no applied stress, the incremental matrix stress, $d\sigma_m$, can be described from Eq. [2] by

$$d\sigma_m = \frac{V_f}{V_f - 1} \times d\sigma_f \quad [20]$$

As the volume fraction of fiber, V_f, lies between 0 and 1, $d\sigma_m$ is negative, while $d\sigma_f$ remains positive. The incremental matrix strain, $d\varepsilon_m$, can be obtained by substituting Eqs. [8], [10], and [20] into [4] as

$$\begin{aligned} d\varepsilon_m = {} & \left[\frac{1}{E_m} + \frac{1}{nK}\left(\frac{\frac{V_f}{V_f - 1} \times \sigma_f - \sigma_{my}}{K}\right)^{\frac{n-1}{n}}\right] \\ & \times \frac{V_f}{V_f - 1} \times d\sigma_f + \alpha_m \times dT \end{aligned} \quad [21]$$

The value of $d\varepsilon_f$ can be obtained by substituting Eqs. [5], [7], and [19] into [3] as

$$d\varepsilon_f = \frac{d\sigma_f}{E_f} + \alpha_f \times dT + d\xi \times \varepsilon^{t\max} \quad [22]$$

By substituting Eqs. [11] or [14], [13] or [16], [17], [18], [21], and [22] into [1], the constitutive equation in terms of fiber stress increment, $d\sigma_f$, is given by

$$\begin{aligned} & \left\{\left[\frac{1}{E_m} + \frac{1}{nK}\left(\frac{\frac{V_f}{V_f - 1} \times \sigma_f - \sigma_{my}}{K}\right)^{\frac{n-1}{n}}\right] \times \frac{V_f}{V_f - 1} \right. \\ & \left. - \frac{1}{E_f(\xi(T, \sigma_f))}\right\} \times d\sigma_f + \left[\alpha_m \right. \\ & \left. - \alpha_f(\xi(T, \sigma_f))\right] \times dT \\ & - d\xi(T, \sigma_f, dT, d\sigma_f) \times \varepsilon^{t\max} = 0 \end{aligned} \quad [23]$$

From this equation, $d\sigma_f$ can be obtained for a given dT by using iteration, and the composite behavior under the thermomechanical process can be analyzed.

In the isothermal process, steps 2 and 4, where $\varepsilon^{\mathrm{CTE}} = 0$, $d\sigma_m$ can be obtained from Eqs. [1] and [10] as a function of composite strain increment $d\varepsilon_c$ by

Table I. Material Properties

Composite Properties	
V_f	0.027, 0.053
6061 Al Properties	
E_m	70 GPa
α_m	23.6×10^{-6}/K
σ_y	35 MPa (−F), 245 MPa (−T6)
K	445 MPa (−F), 85 MPa (−T6)
n	0.49 (−F), 0.2 (−T6)
μ	26.3 GPa
ν	0.33
k	200 MPa
b	2.83×10^{-10} m
TiNi Fiber Properties	
a	0.1 mm
μ^*	23.4 GPa
ν^*	0.43
M_s	288 K
M_f	280 K
A_s	318 K
A_f	329 K
C_A	7.1 MPa/K
C_M	7.7 MPa/K
E_f^{MAR}	26.3 GPa
E_f^{AUS}	67 GPa
α_f^{MAR}	6.6×10^{-6}/K
α_f^{AUS}	11×10^{-6}/K
$\varepsilon^{t\max}$	0.06

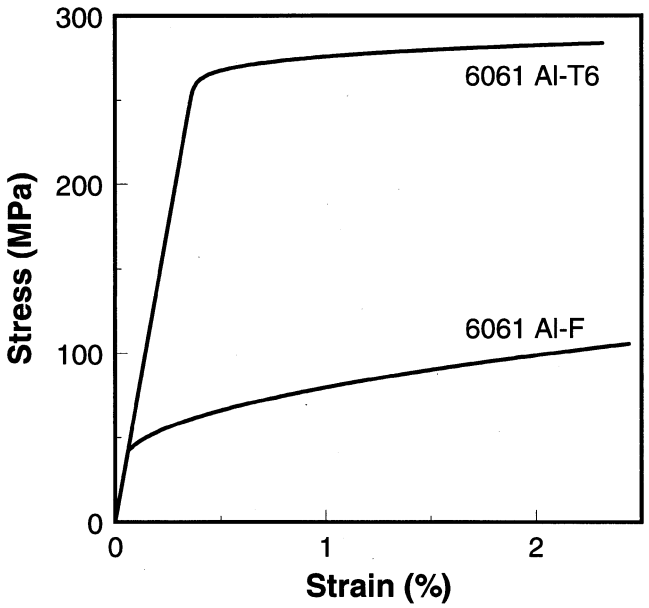

Fig. 6—Stress-strain curves of 6061 Al-T6 and -F.

$$d\sigma_m = \frac{d\varepsilon_c}{\frac{1}{E_m} + \frac{1}{nK}\left(\frac{\sigma_m - \sigma_{my}}{K}\right)^{\frac{n-1}{n}}} \qquad [24]$$

Here, Eqs. [1], [5], [11], or [14], [13] or [16], [18], and [19] are substituted into the incremental form of Eq. [3] as

$$d\varepsilon_c = \frac{d\sigma_f}{E_f\,(\xi(T,\,\sigma_f))} + d\xi(T,\,\sigma_f,\,dT,\,d\sigma_f) \times \varepsilon^{t\max} \qquad [25]$$

Equation [25] provides a correlation between $d\sigma_f$ and $d\varepsilon_c$. Finally, by substituting $d\sigma_f$ and $d\sigma_m$ into Eq. [2], the composite stress increment, $d\sigma_c$, can be solved in terms of $d\varepsilon_c$.

IV. DISCUSSION

The material properties used for the analysis of the thermomechanical process are shown in Table I. The parameters of matrix yield stress and work hardening are measured from the stress-strain curves (Figure 6) of unreinforced matrix specimens, which are processed by the same processing path as the composite.

A. *Cooling Process after Processing or the Heat Treatment (Step 1)*

Since the cooling rate after the hot press of specimens without any heat treatment (graded as F) is so slow, a part of the difference between the press temperature and room temperature can be ignored; *i.e.*, thermal residual stress can be eliminated at the temperature above one-half of the melting temperature (T_m) of the matrix due to a high mobility of matrix dislocations at high temperature. The effective temperature difference, ΔT_{eff}, that would contribute to thermal stresses can be estimated as

$$\Delta T_{\mathrm{eff}} = \frac{1}{2}\,T_m - \mathrm{R}T \qquad [26]$$

In this study, ΔT_{eff} is calculated to about 160 K.

Because the CTE mismatch stress of the fiber in the present composite is calculated to be negative, we need to consider martensitic transformation induced by compressive stress, as reported in other SMA systems.[14,15] This transformation would cause stress relaxation for both the fiber and the matrix in the composite and would reduce residual stress in the matrix, which in turn results in the increase in the composite yield stress in a closer agreement with the experiment. In this study, however, no compressive stress-induced transformation is assumed to occur due to unavailability of the temperature–compression stress phase diagram for this TiNi wire. That is, stress in the fiber during cooling is treated as elastic stress.

B. *Isothermal Loading and Unloading for Prestraining (Step 2)*

Figure 7(a) shows predicted stress-strain curves of TiNi fiber, matrix 6061-F Al, and TiNi/6061 Al-F composite (V_f = 5.3 pct) during loading and unloading.

At the initial part of loading, both TiNi fibers in the austenitic phase and the 6061 Al matrix undergo elastic deformations. Matrix plastic deformation starts when the effective matrix stress reaches its yield stress, while the martensite phase transformation of fibers starts when the fiber stress is equal to the transformation starting stress. In this case, the first kink point of the predicted composite stress-strain curve corresponds to the onset of matrix yielding, and the second kink point to that of the fiber martensite transformation. After loading to a prescribed strain, an elastic unloading takes place. Throughout the prestraining, a prestrain remains in the composite, and the residual stress remains both in the fiber and the matrix. In the unloading

process, the volume fraction of martensite, ξ, remains constant.

Figure 7(b) shows a comparison between predictions and experimental data, where the predictions underestimate the experiment. Two possible reasons for this underestimate are discussed as follows.

One reason is that we assume no fiber phase transformation under compression, as mentioned in Section A (step 1). This neglects the stress relaxation by phase transformation during the cooling process to room temperature, resulting in the overestimation of the matrix tensile and fiber compressive residual stresses, thereby underestimating the composite tensile yield stress.

The second reason is that the dislocation density in the matrix presumably increases as a result of dislocation punching by the CTE mismatch,[16,17,18] which in turn increases the *in situ* yield stress of the matrix in the composite. This increase in the *in situ* yield stress can be estimated by following our previous model on dislocation punching.[17]

The punching distance R is given by

$$R = a\left\{\frac{\frac{\mu}{1-\nu}\alpha^*(1+2\nu+T_1)+\sqrt{Z}}{4k}\right\}^{1/2},$$

$$Z = \left\{\frac{\mu}{1-\nu}\alpha^*(1+2\nu+T_1)\right\}^2 + 16k\frac{\mu}{1-\nu}\alpha^* T_2 \quad [27]$$

where

$$T_1 = \frac{2[\mu^*\{2\nu^*(1-\nu)-\nu\}-\mu\nu(1-2\nu^*)]}{\mu(1-2\nu^*)+\mu^*},$$

$$T_2 = \frac{\mu^*(1-2\nu)-\mu(1-2\nu^*)}{\mu(1-2\nu^*)+\mu^*} \quad [28]$$

Here, a is the radius of fiber, μ and ν are the shear modulus and Poisson's ratio of the matrix, μ^* and ν^* are the shear modulus and Poisson's ratio of fiber, k is the matrix yield stress in shear, and α^* is CTE mismatch and is given by

$$\alpha^* = |(\alpha_f - \alpha_m) \times \Delta T| \quad [29]$$

The dissipation energy W due to the dislocation punching per composite unit volume can be given by

$$W = \frac{4\pi k\alpha^* a^2 \ln(\frac{R}{a})\cdot Vf}{\pi a^2} \quad [30]$$

According to the previous study,[19] approximately a half of the plastic work is used to generate the statistically stored dislocations. The self-energy of a lattice dislocation per unit length is assumed to be $\mu\mathbf{b}^2$, with the Burgers vector of the matrix dislocation being $\mathbf{b}$. The density ρ of the statistically stored dislocations is then given by

$$\rho \cong \frac{\frac{W}{2}}{\mu\mathbf{b}^2} \quad [31]$$

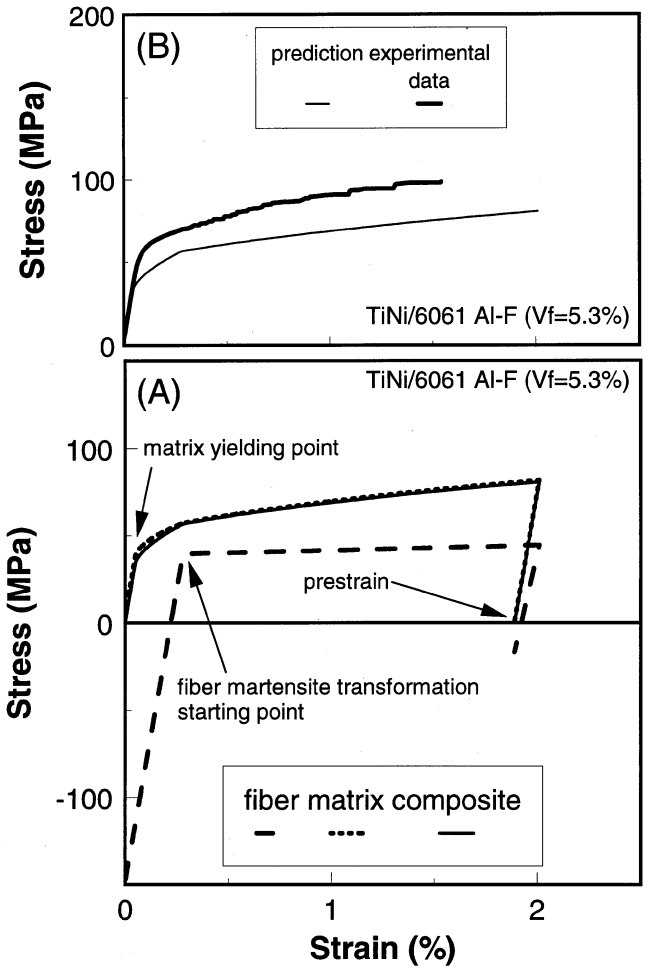

Fig. 7—(*A*) Predictions of fiber, matrix, and applied stress-strain curves of TiNi/6061 Al-F (V_f = 5.3 pct) during prestraining (step 2 in Fig. 2) and (*B*) predictions and experimental data of TiNi/6061 Al-F (V_f = 5.3 pct).

Then, the composite flow stress increment $\Delta\sigma$ is estimated by

$$\Delta\sigma \cong \mu\mathbf{b}\sqrt{\rho} \quad [32]$$

For the Figure 7(b) case, the calculated $\Delta\sigma$ of the TiNi/6061 Al-F composite (V_f = 5.3 pct) is about 19 MPa. If this $\Delta\sigma$ is added to the predicted composite yield stress, the revised predictions are in good agreement with the experiment.

C. *Heating Process (Step 3)*

After the prestraining at room temperature, the composite is heated from 293 to 373 K without applied stress. Figure 8 shows the predicted residual stresses in the fiber and matrix during the heating process. These residual stresses by heating up to the reverse transformation starting point (A_s') are caused by the CTE mismatch between fiber and matrix. At the temperatures above A_s', the fiber stress increases steeply due to the fiber shrinkage caused by the reverse transformation. Figure 8 shows the predicted history of the fiber stress as a function of temperature, where the martensite volume fraction (ξ) at 293 K is 35.6 pct, and it reduces

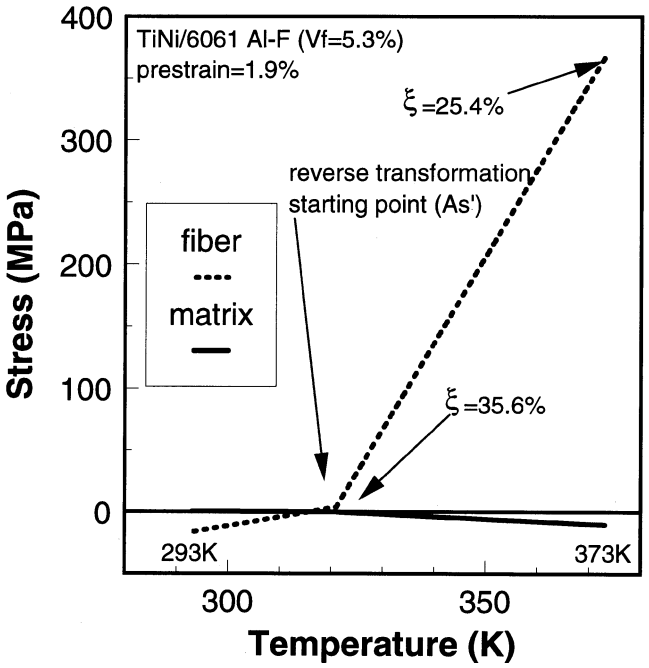

Fig. 8—Predictions of fiber and matrix stress-temperature curves of TiNi/6061 Al-F (V_f = 5.3 pct, prestrain = 1.9 pct) during the heating process (step 3 in Fig. 1).

to 25.4 pct at 373 K. This implies that the martensite phase still remains in the TiNi fiber even at temperatures above A_s. Please note in Figure 8 that the matrix remains compressive, as indicated by the solid line, at 373 K, which will contribute to the increase in the composite yield stress.

D. *Isothermal Tensile Test (Step 4)*

The tensile test of composites is performed at 373 K to obtain a complete set of stress-strain curves from which the composite yield stress (as determined at 0.2 pct off set strain) is measured and plotted as a function of prestrain, as shown in Figure 9. The data show that the composite yield stress increases with an increase in fiber volume fraction and prestrain and that the composite yield stress and work hardening are affected by those of the matrix. Predictions of the composite yield stress based on the present model are also shown by lines in Figure 9, indicating a reasonably good agreement with the experiment, except that the predictions underestimate the experimental data. The main reasons for this underestimate by the present model are already discussed in Section C (step 3), *i.e.*, neglect of possible compressive stress-induced martensite transformation and the increase in the matrix *in situ* yield stress by the dislocation punching.

E. *Interfacial Microstructure*

Interfacial microstructure of the TiNi/Al composites is investigated using scanning electron microscopy (SEM) and energy distribution X-ray (EDX) analysis. Figure 10 shows the SEM images of the interfacial microstructure of the TiNi/6061 Al-F composite processed at three different temperatures: 773, 823, and 873 K. In the composite processed

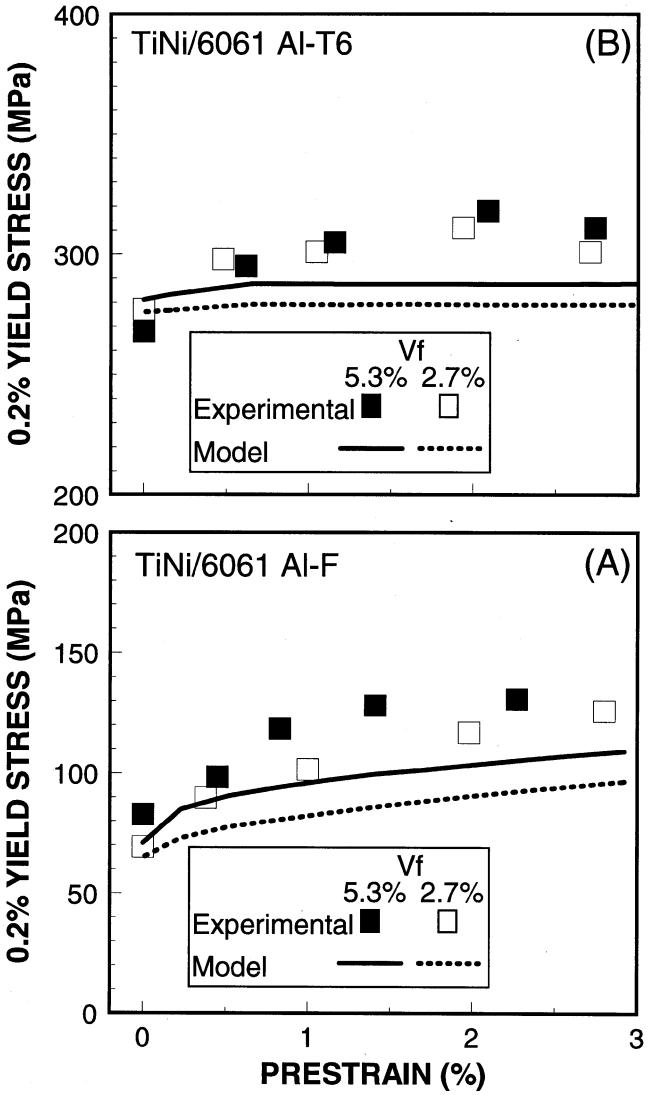

Fig. 9—Experimental data and predictions of the 0.2 pct yield stress dependence on prestrain of (*A*) TiNi/6061 Al-F and (*B*) TiNi/6061 Al-T6 composites.

at 773 K, the interfacial reaction layer observed at the surface of the TiNi fiber is identified as Al_3Ti by the EDX analysis. Since the matrix–side surface of the layer is smoother, this reaction layer appears to have formed on the fiber side. This indicates the diffusion of Al atoms from the matrix into the TiNi fiber. In the composite processed at 823 K, additional reaction particles are observed outside of the Al_3Ti layer, and these particles have grown into the second layer in the composite processed at 873 K. This layer is identified as Al_3Ni by the EDX analysis, indicating that Ni atoms are also diffused from the fiber into the matrix. These two brittle layers of intermetallic compounds are expected to have some influence on the fracture properties of the composite. These brittle layers would be fractured easily during the tensile test, promoting interfacial sliding between the fiber and the matrix. This insufficient stress transfer from the fiber to the matrix with the interfacial sliding is expected to reduce the matrix residual stress,

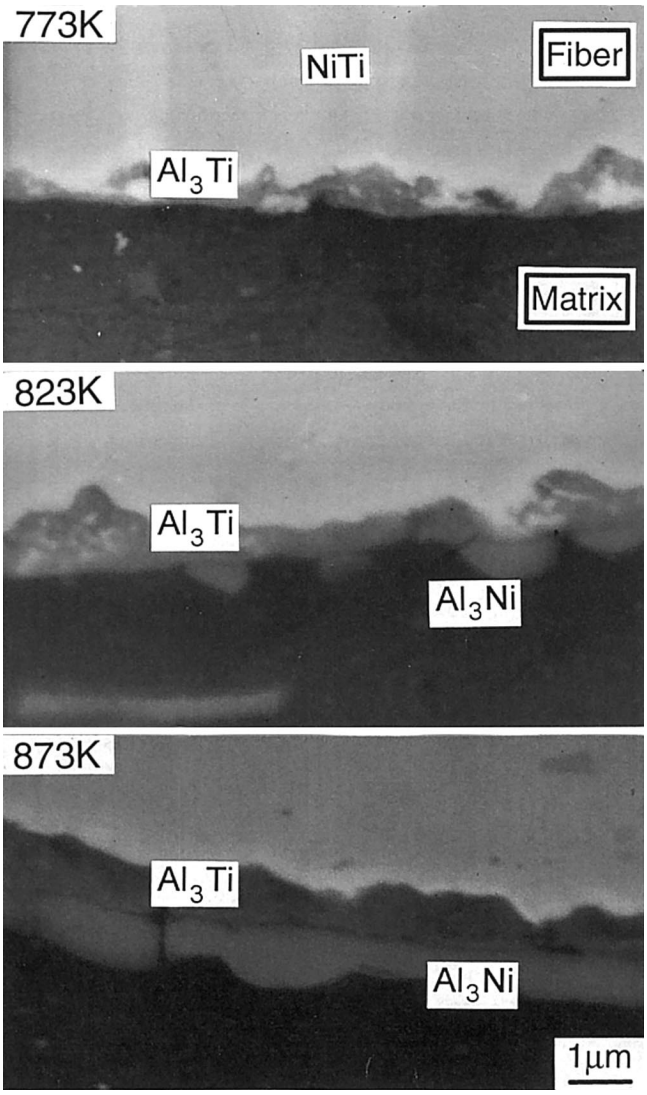

Fig. 10—SEM images of the interfacial microstructure of the TiNi/6061 Al-F composite. The process temperatures are 773, 823, and 873 K.

hence reducing the increase in the composite yield stress at higher temperatures.

V. CONCLUSIONS

The TiNi SMA fiber-reinforced 6061 Al alloy matrix composite with prestrain was successfully processed. As-processed composite was given prestrain at room temperature and heated to the temperature above A_f; then, it was subjected to tensile testing. The measured composite yield stress was observed to increase with prestrain and fiber volume fraction. The dependence of the composite yield stress on prestrain is evaluated by the present model, where an exponential type SMA constitutive equation is used. The main findings of this study are summarized as follows.

1. The compressive residual stress in the matrix of the SMA fiber-reinforced composite can be induced by a specific thermomechanical process. This is partially due to the CTE mismatch between the fiber and the matrix and partially due to the fiber shrinkage during the reverse transformation upon heating to above the A_f temperature. This compressive residual stress of matrix is the key factor to improve the tensile yield stress of the smart composite.
2. The yield stress of TiNi/6061 Al-F and -T6 composites increases with the fiber volume fraction and prestrain increase.
3. Due to the stress increment during reverse transformation, the martensite phase in the fiber can still remain at a temperature higher than A_f.
4. The present model successfully predicts the observed composite yield stress dependency on the fiber volume fraction and prestrain, but underestimates the experiment. The gap between the predicted and experimental composite yield stresses can be explained by the dislocation punching during cooling process.

ACKNOWLEDGMENTS

The authors acknowledge the support of the National Science Foundation, Grant No. CMS-94-9414696, and also thank Dr. J.K. Lee (presently at Hyundai Motor Company, Ulsan, Korea) for his fruitful advice on the model.

TABLE OF SYMBOLS

Composite Constitutive Process Variables	
T	temperature
V_f	volume fraction of fiber
σ_c	composite stress (applied stress)
σ_f, σ_m	stress of fiber and matrix
σ_{fy}, σ_{my}	yield stress of fiber and matrix
ε_c, ε_f, ε_m	strain of composite, fiber, and matrix, respectively
ε^{el}	elastic strain
ε^{pl}	plastic strain
$\varepsilon^{\mathrm{CTT}}$	thermal strain
$\varepsilon^{\mathrm{trans}}$	transformation strain of fiber
E_c, E_f, E_m	elastic modulus of composite, fiber, and matrix, respectively
α_c, α_f, α_m	coefficient of thermal expansion of composite, fiber, and matrix, respectively
K, n	stress constant and stress exponent of matrix work hardening
k, μ, ν	yield stress in shear, shear modulus, and Poisson's ratio of matrix, respectively
b	Burgers vector of matrix
μ^*, ν^*	shear modulus and Poisson's ratio of fiber, respectively
a	radius of fiber
SMA Fiber Constitutive Properties	
ζ	volume fraction of martensite
M_s	austenite to martensite transformation starting temperature under zero stress
M_f	austenite to martensite transformation finishing temperature under zero stress
A_s	martensite to austenite transformation starting temperature under zero stress
A_f	martensite to austenite transformation finishing temperature under zero stress

C_A	slope of the martensite to austenite transformation contours, Fig. 2
C_M	slope of the austenite to martensite transformation contours, Fig. 2
a_M, b_M	austenite to martensite transformation shape parameter
a_A, b_A	martensite to austenite transformation shape parameter
E_f^{MAR}	elastic modulus of the fully martensite fiber
E_f^{AUS}	elastic modulus of the fully austenite fiber
α_f^{MAR}	coefficient of thermal expansion of the fully martensite fiber
α_f^{AUS}	coefficient of thermal expansion of the fully austenite fiber
ε^{tmax}	maximum transformation strain from fully one phase to the fully other phase

REFERENCES

1. M. Taya, Y. Furuya, Y. Yamada, R. Watanabe, S. Shibata, and T. Mori: *Proc. Smart Mater., SPIE*, 1993, pp. 373-83.
2. J.G. Boyd and D.C. Lagoudas: *J. Intell. Mater. Systems Struct.*, 1994, vol. 5, pp. 333-46.
3. Y. Furuya, A. Sasaki, and M. Taya: *Mater. Trans., JIM*, 1993, vol. 34, pp. 224-27.
4. W.D. Armstrong: *J. Intell. Mater. Systems Struct.*, 1996, vol. 7, pp. 448-54.
5. M. Taya, A. Shimamoto, and Y. Furuya: *Proc. 10th Int. Conf. of Composite Materials*, 1996, vol. V, pp. 275-82.
6. For example, K. Otsuka, C.M. Wayman, K. Nakai, H. Sakamoto, and K. Shimizu: *Acta Metall.*, 1976, vol. 24, pp. 207-26.
7. T. Mori and K. Tanaka: *Acta Metall.*, 1973, vol. 21, pp. 571-74.
8. K. Tanaka: *Res Mechanica*, 1986, vol. 18, pp. 251-63.
9. W.D. Armstrong and H. Kino: *J. Intell. Mater. Systems Struct.*, 1995, vol. 6, pp. 809-16.
10. W.D. Armstrong: *J. Intell. Mater. Systems Struct.*, 1996, vol. 7, pp. 448-54.
11. C. Liang and C.A. Rogers: *J. Intell. Mater. Systems Struct.*, 1990, vol. 1, pp. 207-34.
12. L. Brinson: *J. Intell. Mater. Systems Struct.*, 1993, pp. 229-42.
13. D.S. Ford and S.R. White: *Acta Mater.*, 1996, vol. 44, pp. 2295-2307.
14. L. Orgeas and D. Favier: *J. Phys. IV (Coll.)*, 1995, vol. 5 (C8), pt. 2, pp. 605-10.
15. V. Novak, J. Malimanek, and N. Zarubova: *J. Phys. IV (Coll.)*, 1995, vol. 5 (C8), pt. 2, pp. 997-1002.
16. M. Vogelsang, R.M. Fisher, and R.J. Arsenault: *Metall. Trans. A*, 1986, vol. 17A, pp. 379-89.
17. S. Shibata, T. Mori, and M. Taya: *Scripta Metall. Mater.*, 1992, vol. 26, pp. 363-68.
18. D.C. Dunand and A. Mortensen: *Acta Metall.*, 1991, vol. 39, pp. 1405-16.
19. C.T. Kim, J.K. Lee, and M.R. Plichta: *Metall. Trans. A*, 1990, vol. 21A, pp. 673-82.